Energy spectra in elasto-inertial turbulence

P. C. Valente, C. B. da Silva, and F. T. Pinho

Citation: Physics of Fluids **28**, 075108 (2016); doi: 10.1063/1.4955102
View online: http://dx.doi.org/10.1063/1.4955102
View Table of Contents: http://scitation.aip.org/content/aip/journal/pof2/28/7?ver=pdfcov
Published by the AIP Publishing

Articles you may be interested in

Elasto-inertial particle focusing under the viscoelastic flow of DNA solution in a square channel
Biomicrofluidics **10**, 024111 (2016); 10.1063/1.4944628

On the mechanism of elasto-inertial turbulence
Phys. Fluids **25**, 110817 (2013); 10.1063/1.4820142

Effects of viscoelasticity on the probability density functions in turbulent channel flow
Phys. Fluids **21**, 115106 (2009); 10.1063/1.3258758

Characteristic scales and drag reduction evaluation in turbulent channel flow of nonconstant viscosity viscoelastic fluids
Phys. Fluids **16**, 1581 (2004); 10.1063/1.1689971

Budgets of Reynolds stress, kinetic energy and streamwise enstrophy in viscoelastic turbulent channel flow
Phys. Fluids **13**, 1016 (2001); 10.1063/1.1345882

Reuse of AIP Publishing content is subject to the terms at: https://publishing.aip.org/authors/rights-and-permissions. Downloaded to IP: 193.136.33.229 On: Fri, 22 Jul 2016 15:24:55

CrossMark click for updates

PHYSICS OF FLUIDS **28**, 075108 (2016)

Energy spectra in elasto-inertial turbulence

P. C. Valente,[1] C. B. da Silva,[1] and F. T. Pinho[2]
[1]*IDMEC/IST, University of Lisbon, Ave. Rovisco Pais, 1049-001 Lisboa, Portugal*
[2]*CEFT/FEUP, University of Porto, Rua Dr. Roberto Frias, 4200-465 Porto, Portugal*

(Received 17 May 2016; accepted 20 June 2016; published online 22 July 2016)

Direct numerical simulations of statistically steady homogeneous isotropic turbulence in viscoelastic fluids described by the FENE-P model are presented. Emphasis is given to large polymer relaxation times compared to the eddy turnover time, which is a regime recently termed elasto-inertial turbulence. In this regime the polymers are ineffective in dissipating kinetic energy but they play a lead role in transferring kinetic energy to the small solvent scales which turns out to be concomitant with the depletion of the usual non-linear energy cascade. However, we show that the non-linear interactions are still highly active, but they lead to no net downscale energy transfer because the forward and reversed energy cascades are nearly balanced. Finally, we show that the tendency for a steeper elasto-inertial power-law spectra is reversed for large polymer relaxation times and the spectra tend towards the usual $k^{-5/3}$ functional form. *Published by AIP Publishing.* [http://dx.doi.org/10.1063/1.4955102]

I. INTRODUCTION

The addition of small amounts of macromolecules, or of surfactants that form large worm-like micelles, to an otherwise Newtonian solvent imparts a complex rheological behavior to the fluid, and in particular viscoelasticity. These solutions exhibit dramatically different turbulent flow characteristics, relative to those of the solvent, leading to such changes as a substantial reduction of wall friction.[1,2] The corresponding topological modifications of the turbulent structures are a consequence of the evolution of the additional stresses brought by the additives, henceforth denoted as polymer stresses, as the polymers stretch and recoil, and which can be of the order of the stresses caused by the turbulence itself.[1–5] This remarkable discovery has motivated many investigations of polymer-laden turbulence, particularly in wall-bounded flows due to the industrial applications of this technology in reducing pumping and heat transfer losses in pipelines and district heating/cooling systems.[2,6]

One of the early findings in wall turbulence of viscoelastic fluids is that the drag reduction increases up to a maximum asymptote, usually denoted as maximum drag reduction asymptote or Virk's asymptote.[1,2,5] The maximum drag reduction regime is observed when the relaxation time of the polymer solutions is large with respect to the turbulence time scales and the shear time scales of the gradient imposed by the wall.[7,8] This regime has been recently termed elasto-inertial turbulence[8,9] due to the strong interactions between the inertial and the elastic degrees of freedom.

The effect of fluid elasticity upon wall-free turbulence, and in particular on homogeneous turbulence, has received substantial less attention given its apparently looser connection with industrial applications. Simultaneously, it is not clear that the physical mechanisms causing drag reduction in wall turbulence are present in polymer-laden homogeneous turbulence.[5] Therefore, although drag reduction in duct flows is currently the main application of polymer-laden flows, there is great potential for using polymers, and especially degradation-resisting surfactants, in other industrial applications where the walls play a secondary role[10–12] as in jet mixing systems. Furthermore, to make significant progress in the development of turbulence models, even for wall-bounded turbulent flows, it is unavoidable to use homogeneous turbulence as a benchmark in order to focus on an essential part of any turbulence model—the model for the non-linear energy cascade. The development of advanced turbulence models for viscoelastic fluid flows is precisely one of our ultimate

Reuse of AIP Publishing content is subject to the terms at: https://publishing.aip.org/authors/rights-and-permissions. Downloaded to IP: 193.136.33.229 On: Fri, 22 Jul 2016 15:24:55

goals and it is instructive to realize that in one of the few attempts to produce a model for large-eddy simulations of polymer-laden turbulence[13,14] emphasis was given on modelling the unresolved part of the polymer conformation tensor, but the effect of the polymers on the sub-grid stresses, so relevant in the momentum balance, was neglected. We argue that this is due to the lack of physical knowledge on the effect of the polymers on the non-linear energy cascade for a wide range of values of the ratio between the polymer relaxation time over the turbulence time scale. Here we aim to contribute to the physical understanding of the effect of the polymers on the non-linear energy cascade and on the kinetic energy spectrum with emphasis on the large polymer relaxation time regime, i.e., for elasto-inertial turbulence.

In our previous work on forced homogeneous turbulence of viscoelastic fluids[15] represented by the finitely extensible nonlinear elastic model with the Peterlin approximation (FENE-P) direct numerical simulations (DNSs) were used to show that as the polymer relaxation time increases, the transfer of kinetic to elastic energy occurs at decreasingly smaller wavenumbers (i.e., at larger scales). As the polymer relaxation time was further increased, the energy removed by the polymers at the large scales surpassed the energy that the polymers dissipated and the extra energy was injected back to the turbulence at high wavenumbers, which is effectively a polymer-induced kinetic energy cascade. This additional kinetic energy cascade is an alternative route to transfer energy from large to small scales which competes with the usual non-linear energy cascade leading to its depletion. We now complement the existing data with new DNS data for significantly larger polymer relaxation times, as compared to the turnover time of turbulence, and investigate turbulence dynamics and the polymer-turbulence interactions. It is shown that the severe reduction of the net nonlinear energy cascade is due not only to the reduction of forward scatter, but also to a large extent to the increase of backscatter, which becomes nearly balanced with the forward scatter. We also investigate the shape of the kinetic energy spectra, in particular the dichotomy between Kolmogorov's $k^{-5/3}$ inertial range and other steeper power-laws predicted by viscoelastic theories[3,16] and reported in previous studies[17,18] and show that the latter only exist within an intermediate range of Deborah numbers (the Deborah number De is the ratio between the polymer relaxation time and the eddy turnover time scale), whereas the $-5/3$ law is encountered at small and very large values of De.

The remainder of this paper is organized as follows: after briefly presenting the governing equations and the numerical methods, the whole set of DNS data is introduced at the beginning of Section III followed by its detailed discussion in the remainder of Section III and in Section IV. A summary of the main findings closes the paper.

II. GOVERNING EQUATIONS AND METHODS

The rheological behaviour of the polymer solutions is represented by the finitely extensible non-linear elastic continuous model closed with the Peterlin approximation.[19,20] The FENE-P has three parameters: the (longest) relaxation time τ of the polymer molecules, its maximum (squared) extensibility L^2 (which is normalised by the square of the equilibrium radius $\langle R^2\rangle_0$ of the polymer chain), and the zero-shear-rate kinematic viscosity coefficient $\nu^{[p]}$. The zero-shear-rate viscosity is included in the model as a non-dimensional parameter β which is the ratio between the solvent and the total zero-shear-rate viscosity of the solution ($\beta \equiv \nu^{[s]}/(\nu^{[p]}+\nu^{[s]})$). The dumbbells are represented as a continuous tensor field, the conformation tensor, which is defined as the normalised second moment of the end-to-end vector of the dumbbell separation $\mathbf{r}$, $C_{ij} \equiv \langle r_i r_j\rangle/\langle R^2\rangle_0$, where the brackets "$\langle\rangle$" represent an averaging operation (the subscript index $i = 1, 2, 3$ represents the three components of the local coordinate system). The polymers cause additional stresses in the momentum transport equations which are computed from the conformation tensor as $\sigma_{ij}^{[p]} = \frac{\rho\,\nu^{[p]}}{\tau}\left[f(C_{kk})C_{ij} - \delta_{ij}\right]$ (summation over repeated indices implied; ρ is the density of the fluid, $f(C_{kk}) \equiv (L^2-3)/(L^2-C_{kk})$ is the Peterlin function, u_i, with i = 1,2, or 3 are the three zero-mean fluctuating components of the velocity vector field and δ_{ij} is the identity matrix). As in Valente *et al.*,[15] the incompressible momentum transport equations are integrated in a triple periodic domain with N collocation points using a pseudo-spectral method (de-aliased with the 2/3 rule) and a third-order Runge-Kutta scheme in time. The transport equation for the conformation tensor is

Reuse of AIP Publishing content is subject to the terms at: https://publishing.aip.org/authors/rights-and-permissions. Downloaded to IP: 193.136.33.229 On: Fri, 22 Jul 2016 15:24:55

solved using the central differences algorithm proposed by Vaithianathan *et al.*[21] based on the Kurganov-Tadmor method, which guarantees that the conformation tensor remains symmetric and positive definite. In the present simulations the turbulence is sustained by an artificial forcing delta-correlated in time and uncorrelated with the velocity field[22] with a prescribed power input spectrum $f(k)$ (and thus a prescribed total power input P). The chosen power input spectrum is a Gaussian profile centred at wavenumber 3 and distributed over the neighbouring wavenumbers 2 and 4 which leads to a ratio between the box size and the integral scale between 9 and 14. We note in passing that different large scale forcing parameters were also tested with no meaningful impact on the results.[15] Further details on the transport equations and numerical methods used to integrate them can be found in Valente *et al.*[15]

We also perform simulations with a higher-order viscous term, $(-1)^{h+1}\nu^{[h]}\Delta^h u_i$, where h and $\nu^{[h]}$ are the order of the hyperviscosity and the corresponding hyperviscosity coefficient.[23,24] Direct numerical simulations with hyperviscosity have been widely used to study inertial range statistics of periodic box turbulence in Newtonian fluids by taking advantage of the fact that increasing the order of the dissipative term concentrates the dissipation onto a narrower band of large wavenumbers and consequently increases the extent of the inertial range.[23–25] This technique has also been applied to study turbulence subjected to rotation[26,27] and stratification[27,28] as well as magnetohydrodynamic turbulence[29] to name but a few examples. However, as far as the authors are aware, this is the first time that hyper-viscous simulations are used to study polymer-laden turbulent flows. We set $h = 4$ for all our hyperviscous simulations and we use a criterion for the choice of $\nu^{[h]}$ similar to that proposed by Borue and Orszag,[24] specifically, $\nu^{[h]} \approx 0.5((N-2)/2)^{-2h}/\delta t$, where δt is the time step of the numerical scheme. Since this choice of hyperviscosity coefficient is not necessarily adequate for viscoelastic hyperviscous simulations, we confirmed that the roll-off of the spectra was sufficiently fast so that the power removed by hyperviscous dissipation between the two largest resolved wavenumbers was negligible. It is important to note that the non-dimensional parameter β has no immediate counterpart in hyperviscous simulations and therefore we chose to directly set the zero-shear-rate polymer viscosity $\nu^{[p]}$ to be equal to that of the remaining simulations. However, this implies that quantitative comparisons of global statistical quantities such as fraction of power dissipated by the solvent and by the polymers are not meaningful. In any case, we are solely interested in qualitative information on the behaviour of the spectra which are at most complementary to the main data presented in this paper.

The turbulent kinetic energy K, the Newtonian solvent dissipation $\varepsilon^{[s]}$, and the integral scale ℓ are extracted from the kinetic energy spectrum $E(k)$ in the usual way[15]: $K = \sum_k E(k)$, $\varepsilon^{[s]} = 2\nu^{[s]} \sum_k k^2 E(k)$ and $\ell = \pi/(2K) \sum_k E(k)/k$, and the kinetic energy spectrum is computed as

$$E(k) = 4\pi k^2 \left\langle \frac{1}{2}\widehat{u}_i(\vec{k},t)\widehat{u}_i^*(\vec{k},t) \right\rangle_{|\vec{k}|}, \tag{1}$$

where $\widehat{u}_i(\vec{k},t) = FFT\left\{u_i(\vec{x},t)\right\}$ is the Fourier coefficient of the velocity field $u_i(\vec{x},t)$ and "$*$" represents a complex conjugate (FFT is the direct Fourier transform operation), while

$$\left\langle \widehat{\phi}(\vec{k},t) \right\rangle_{|\vec{k}|} = \frac{1}{N_k} \sum_{k-\frac{\Delta k}{2} < |\vec{k}| < k+\frac{\Delta k}{2}} \widehat{\phi}(\vec{k},t) \tag{2}$$

denotes a spherical-shell average of the quantity $\widehat{\phi}$ over N_k modes in the shell, of thickness Δk, centred at k.

These quantities are used to define the Taylor microscale $\lambda \equiv \sqrt{10\nu^{[s]}K/\varepsilon^{[s]}}$, the Kolmogorov length-scale $\eta \equiv (\nu^{[s]3}/\varepsilon^{[s]})^{1/4}$, the eddy turnover time $\ell/\sqrt{K}$, the Taylor microscale based Reynolds number, $Re_\lambda \equiv \sqrt{(2/3)K}\,\lambda/\nu^{[s]}$, and the integral scale based Reynolds number, $Re_\ell \equiv \sqrt{(2/3)K}\,\ell/\nu^{[s]}$. Since the turbulence is statistically homogeneous and stationary, the volume-averaged kinetic energy converted to elastic energy—given by the work of polymer stress against the strain rate $\left\langle \sigma_{ij}^{[p]} S_{ij} \right\rangle$—is equal to the average elastic energy dissipated by the polymers, i.e., $\varepsilon^{[p]} \equiv \left\langle f(C_{ii})\sigma_{jj}^{[p]} \right\rangle /2\tau = \left\langle \sigma_{ij}^{[p]} S_{ij} \right\rangle$ (recall that "$\langle\rangle$" indicates an average over the computation domain). We also define a Deborah number, $\mathrm{De} \equiv \tau\sqrt{K}/\ell$, representing the ratio between the relaxation time and the eddy turnover time scale,

Reuse of AIP Publishing content is subject to the terms at: https://publishing.aip.org/authors/rights-and-permissions. Downloaded to IP: 193.136.33.229 On: Fri, 22 Jul 2016 15:24:55

and a Weissenberg number, $\mathrm{Wi} \equiv \tau/\tau_\eta$, representing the ratio between the relaxation and Kolmogorov time scales. We compute Lumley's length scale[4] r_L and the corresponding wavenumber $k_L = r_L^{-1}$ from the crossover between the local eddy turnover time and the relaxation time of the polymer (see Sec. 2 of Ref. 15 for further details on the methodology to obtain r_L). Note that in Valente *et al.*[15] we computed the corresponding wavenumber as $k_L = 2\pi/r_L$ such that $r_L = 2\pi$ would imply a Lumley scale of the size of the box size, but we opted to remove the 2π factor here following Refs. 18 and 30.

III. HIGH DEBORAH NUMBER VISCOELASTIC TURBULENCE

We start by further extending the range of Deborah numbers straddled by our DNSs of viscoelastic homogeneous isotropic turbulence up to $De \approx 16$ ($0.1 \leq De \leq 2$ in our previous work[15]). Specifically, we perform four additional simulations with $N = 192^3$ collocation points and the polymer relaxation times set to $\tau = [1.2, 2.0, 3.0, 5.0]$ s, respectively, one simulation with $N = 384^3$ collocation points and $\tau = 2.0$ s, and one with $N = 768^3$ collocation points and $\tau = 0.27$ s (see Table I for further details). For all the simulations presented here, the dimensionless concentration parameter is set to $\beta = 0.8$ as we solely focus on the effect of the polymer relaxation time. These new data are compared with lower Deborah number datasets for the same concentration parameter, especifically datasets 1–11 and 16–18 presented in Table I. Note that for the new DNS data, the maximum extensibility of the polymers is

TABLE I. Compilation of the viscoelastic DNS results. We use S.I. units of the presented quantities considering the box size of the simulations to be $L_{\mathrm{box}} = 2\pi$ [m]. For the $N = 192^3$ simulations (datasets # 1–15) the solvent viscosity is set to $\nu^{[s]} = 0.008$ m^2/s, whereas for the $N = 384^3$ simulations (datasets # 16–19) the solvent viscosity is $\nu^{[s]} = 0.003$ m^2/s. For the dataset # 20 with $N = 768^3$ the solvent viscosity is $\nu^{[s]} = 0.001$ m^2/s. For the hyper-viscous simulations (datasets # 21–26) the zero-shear-rate viscosity of the polymers is set to $\nu^{[p]} = 0.002$ m^2/s. For all the simulations the power input is $P = 3.3$ m^2/s^3 and $\beta = 0.8$. For the new data (datasets # 12–15 and 19–26), $L^2 = 1000^2$, whereas for datasets # 1 – 11, 16 and 17, $L^2 = 100^2$ and for dataset # 18, $L^2 = 150^2$. For the hyper-viscous DNSs we do not define quantities that depend on small-scale statistics.

#	N	Wi (-)	De (-)	Re_λ (-)	K (m^2/s^2)	$\varepsilon^{[s]}$ (m^2/s^3)	$\varepsilon^{[p]}$ (m^2/s^3)	ℓ (m)	λ (m)	$k_{\max}\eta$ (-)	$\langle C_{ii}\rangle/L^2$ (%)	Notes
1	192^3	0.5	0.10	68	3.85	2.67	0.62	0.52	0.34	1.3	0.0	Reference 15
2	192^3	0.9	0.19	67	3.78	2.66	0.63	0.51	0.34	1.3	0.0	Reference 15
3	192^3	1.6	0.35	71	3.64	2.16	1.11	0.54	0.37	1.4	0.1	Reference 15
4	192^3	2.3	0.56	82	2.88	1.02	2.25	0.61	0.47	1.7	1.0	Reference 15
5	192^3	2.7	0.71	79	2.20	0.65	2.70	0.63	0.52	1.9	2.3	Reference 15
6	192^3	3.3	0.84	72	1.82	0.54	2.74	0.64	0.52	2.0	3.9	Reference 15
7	192^3	4.0	0.99	63	1.58	0.52	2.79	0.63	0.49	2.0	5.8	Reference 15
8	192^3	5.1	1.17	59	1.57	0.58	2.70	0.64	0.46	2.0	7.6	Reference 15
9	192^3	5.3	1.20	54	1.48	0.63	2.67	0.61	0.43	1.9	0.1	Reference 15
10	192^3	7.5	1.63	51	1.48	0.70	2.56	0.60	0.41	1.9	11.5	Reference 15
11	192^3	10.2	2.14	47	1.49	0.84	2.46	0.57	0.38	1.8	15.0	Reference 15
12	192^3	14.3	2.95	47	1.73	1.14	2.22	0.53	0.35	1.7	0.3	New
13	192^3	28.3	5.47	50	2.21	1.60	1.77	0.54	0.33	1.5	0.7	New
14	192^3	45.9	9.12	53	2.51	1.88	1.38	0.52	0.33	1.5	1.3	New
15	192^3	80.9	16.2	55	2.73	2.10	1.12	0.51	0.32	1.4	2.4	New
16	384^3	2.9	0.62	183	3.04	0.61	2.73	0.56	0.39	1.9	2.7	Reference 15
17	384^3	4.1	0.91	160	1.92	0.32	2.89	0.61	0.43	2.2	7.6	Reference 15
18	384^3	10.5	1.71	98	1.50	0.52	2.87	0.57	0.29	1.9	13.1	Reference 15
19	384^3	45.3	6.71	100	2.63	1.54	1.85	0.48	0.23	1.5	2.0	New
20	768^3	4.5	0.75	391	2.54	0.28	2.99	0.58	0.30	2.0	0.2	New
21	192^3	…	0.11	…	4.07	…	1.52	0.46	…	…	0.0	New (hyperviscous)
22	192^3	…	0.37	…	3.73	…	2.86	0.53	…	…	0.0	New (hyperviscous)
23	192^3	…	0.57	…	2.81	…	3.16	0.59	…	…	0.0	New (hyperviscous)
24	192^3	…	0.86	…	1.77	…	3.24	0.62	…	…	0.0	New (hyperviscous)
25	192^3	…	1.84	…	1.59	…	3.15	0.55	…	…	0.1	New (hyperviscous)
26	192^3	…	7.13	…	2.84	…	2.70	0.47	…	…	1.0	New (hyperviscous)

Reuse of AIP Publishing content is subject to the terms at: https://publishing.aip.org/authors/rights-and-permissions. Downloaded to IP: 193.136.33.229 On: Fri, 22 Jul 2016 15:24:55

set to $L^2 = 1000^2$, which is much larger than that used in the previous DNSs ($L^2 \leq 150^2$). We use a larger L^2 in order to ensure that the polymers are operating in the linear elastic regime and to avoid confounding effects in this first attempt to understand the behaviour of the energy spectra and of the kinetic energy cascades as we increase the Deborah number.

To the best of our knowledge, the Deborah numbers straddled by our data far exceed those previously assessed in laboratory and numerical experiments of turbulent flows not bounded by walls and therefore the careful reader may question the physical relevance of the present data in the absence of experimental observation. We have two complementing viewpoints on this issue. On the one hand, the response of the energy cascade to the additional degrees of freedom and its consequence on the power-law range of the energy spectra that we report on Secs. III A and III B are very pertinent to the general understanding of turbulence phenomena in itself, even if this regime of inertio-elastic turbulence is not so easily realizable in experiments due to, e.g., polymer degradation. On the other hand, we believe that this regime of large De is realizable in carefully designed experiments as explained below. One of the main experimental limitations in polymer-laden turbulence is mechanical polymer degradation which hinders, e.g., experimental repeatability. If one is to design such an experiment, one of the primary concerns would be to ensure that the polymers are not extended in excess, say, less than 1/3 of the maximum extensibility, on average. According to our data, this condition could be satisfied even for a Deborah number higher than that of our set #17 ($De \approx 0.9$ and $Re_\lambda \approx 160$ or $Re_\ell \approx 230$, cf. Table I), up to $De \approx 10$. Such an experiment could rely on the same high molecular weight polyacrylamide (PAAm; $M = 1.8 \times 10^7$ Da) as used by Ouellette *et al.*,[31] which is characterized by $L^2 = 150^2$ ($L^2 = 3Q_0^2/(6R_g^2)$, Q_0—length of fully extended chain, R_G—radius of gyration[32]) up to concentrations within the dilute regime ($c^\star \approx 200$ ppm for this PAAm[33]). To match De and Re_λ or Re_ℓ in the experiment, one can adjust the solvent viscosity and the polymer relaxation time for given turbulence parameters ℓ and K (note that the relaxation time depends on the viscosity of the solvent according to the Zimm model for infinite dilution,[31,33] $\tau_0 = \nu^{[s]} R_G^3/(\rho k_B T)$ and on the concentration[33] following $\tau/\tau_0 = 1 + cA - \sqrt{2}(cA)^{3/2} + 2(cA)^2$, where R_G, k_B, T, c, and A are gyration radius, Boltzmann's constant, temperature of the solution, concentration in SI units and A is related to the intrinsic viscosity[33]). The viscosity of water can be increased by up to two orders of magnitude by suitable addition of sorbitol and sucrose.[33] For example, for values of $\ell \approx 10$ cm and $\sqrt{K} \approx 0.1$ m/s, of the order of those reported by Ouellette *et al.*,[31] one could obtain $De \approx 2$ and $Re_\lambda \approx 100$ by setting the solvent viscosity to roughly $\nu^{[s]} = 5 \times 10^{-6}$ m^2/s (the estimated relaxation time is $\tau = 0.55$ s for $c \approx c^\star$). By doubling the solvent viscosity one could reach $De \approx 3$, while keeping Re_λ of the same order. If the solvent viscosity is raised to $\nu^{[s]} = 5 \times 10^{-5}$ m^2/s and the polymer concentration is raised above the overlap concentration in the semi-dilute unentangled regime, then $De \approx 10$ and $Re_\lambda \approx 50$. Although for increasing De we expect the extensibility of the polymer to increase,[15] and hence the polymer degradation to worsen, this can be offset by the increase in polymer concentration which leads to smaller extensibilities.[15] Finally, note that higher values of Re_λ can be reached with higher values of K, well within the range of velocity scales attainable in tank and/or water flume experiments ($\ell = [1\text{–}10]$ cm and $\sqrt{K} = [0.05\text{–}0.4]$ m/s).

A. Non-linear energy cascade versus polymer induced energy cascade

We continue this study by analysing the energy cascade mechanisms for the new high Deborah number simulations, which complement the previous simulations and allow a more complete analysis of the interplay between inertial and elastic degrees of freedom for a wide range of Deborah numbers. As in Valente *et al.*[15] the energy cascade mechanism is investigated by analysing the scale-by-scale kinetic energy budget in wavenumber space using a Lin-type equation[34,35] modified to include the kinetic energy transfer between the solvent and the polymers,

$$\frac{\partial E(k,t)}{\partial t} = T(k,t) - T^{[p]}(k,t) - 2\nu^{[s]}k^2E(k,t) + f(k,t), \tag{3}$$

where $E(k,t)$ is the kinetic energy spectrum, while $2\nu^{[s]}k^2E(k)$ and $f(k,t)$ represent the viscous dissipation and energy input (caused by the forcing) within the solvent at wavenumber k,

Reuse of AIP Publishing content is subject to the terms at: https://publishing.aip.org/authors/rights-and-permissions. Downloaded to IP: 193.136.33.229 On: Fri, 22 Jul 2016 15:24:55

respectively. $T(k,t)$ and $T^{[p]}(k,t)$ represent transfers of kinetic energy across wavenumber k within the solvent and between the solvent and polymer molecules, respectively. Specifically, positive/negative values of $T(k,t)$ represent kinetic energy transfer within the solvent from wave numbers smaller than k into/from wave numbers larger than k. Similarly, positive/negative values of $T^{[p]}(k,t)$ represent a transfer of kinetic energy into/from the polymer molecules.

The non-linear kinetic energy transfer at wavenumber k is described by the function,

$$\widehat{T}(\vec{k},t) = \Re\left\{\widehat{u}_i^*(\vec{k},t)\widehat{N}_i(\vec{k},t)\right\}, \tag{4}$$

where $\widehat{N}_i(\vec{k},t) = \mathrm{i}k_j\widehat{u_iu_j}(\vec{k},t)$ is the non-linear term of the Navier-Stokes equations, and $\Re$ denotes the real part of the term inside brackets ($i = \sqrt{-1}$). The spectral kinetic energy transfer function $T(k,t)$, representing the non-linear kinetic energy transfer at wavenumber k, is obtained by spherical shell-averaging this quantity,

$$T(k,t) = 4\pi k^2\left\langle\widehat{T}(\vec{k},t)\right\rangle_{|\vec{k}|}, \tag{5}$$

while the transfer of kinetic energy between the solvent and the polymer molecules at wavenumber k described by term $T^{[p]}(k,t)$ is computed by shell-averaging the energy transfer between solvent and polymer at wavenumber vector $\vec{k}$ (see Refs. 15 and 36–38),

$$T^{[p]}(k,t) = 4\pi k^2\left\langle\widehat{S}_{ij}^*(\vec{k},t)\widehat{\sigma}_{ij}^{[p]}(\vec{k},t) + \widehat{S}_{ij}(\vec{k},t)\widehat{\sigma}_{ij}^{[p]*}(\vec{k},t)\right\rangle_{|\vec{k}|} = 8\pi k^2\left\langle\Re\left\{\widehat{S}_{ij}^*(\vec{k},t)\widehat{\sigma}_{ij}^{[p]}(\vec{k},t)\right\}\right\rangle_{|\vec{k}|}, \tag{6}$$

where $S_{ij} = 1/2\left(\partial u_i/\partial x_j + \partial u_j/\partial x_i\right)$ is the rate-of-strain tensor.

Since the flow is statistically stationary, Equation (3) becomes

$$f(k) = -T(k) + T^{[p]}(k) + 2\nu^{[s]}k^2E(k). \tag{7}$$

Integrating each term in Eq. (7) from 0 to k we get

$$F(k) = \Pi(k) + \Pi^{[p]}(k) + D(k), \tag{8}$$

where each term represents the same physical mechanisms as in Eq. (7), integrated up to wavenumber k, e.g., $\Pi^{[p]}(k) \equiv \sum_{k''<=k} T^{[p]}(k'')$. Note, however, the sign swap of the term $\Pi(k) \equiv -\sum_{k''<=k} T(k'')$, so that it is a positive quantity for a downscale energy flux. From these quantities one can compute the total solvent dissipation, and total polymer dissipation as $\varepsilon^{[s]} = D(k_{max}) = 2\nu^{[s]}\sum_k k^2 E(k)$, and $\varepsilon^{[p]} = \sum_k T^{[p]}(k)$, respectively, while the total power input is $P = F(k_{max}) = \sum_k f(k)$. In the present work, since we are dealing with a statistically stationary flow, the total power input from the forcing is equal to the sum of the solvent and polymer dissipations, i.e., $P = \varepsilon^{[s]} + \varepsilon^{[p]}$.

Figure 1(a) shows the fraction of the total power input dissipated by the solvent $\varepsilon^{[s]}/P$, and dissipated by the polymers $\varepsilon^{[p]}/P$, and complements Fig. 2(a) from Valente *et al.*[15] For the smaller

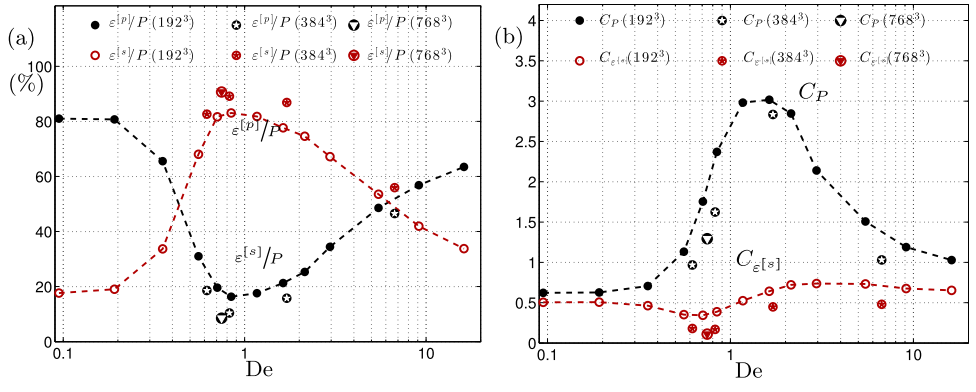

FIG. 1. (a) Fraction of the power input P dissipated by the solvent $\varepsilon^{[s]}/P$, and by the polymers, $\varepsilon^{[p]}/P$ as a function of the Deborah number. (b) Normalised solvent dissipation, $C_{\varepsilon[s]} \equiv (3/2)^{5/2}\varepsilon^{[s]}\ell/K^{3/2}$ and normalised total power dissipated $C_P \equiv (3/2)^{5/2}P\,\ell/K^{3/2}$, as function of the Deborah number. Data for both the lower and larger Reynolds numbers are identified by the number of collocation points used in the simulations (see Table I).

Reuse of AIP Publishing content is subject to the terms at: https://publishing.aip.org/authors/rights-and-permissions. Downloaded to IP: 193.136.33.229 On: Fri, 22 Jul 2016 15:24:55

Deborah numbers ($De \ll 1$) most of the dissipation is caused by the solvent (~80%, which is consistent with $\beta = 0.8$), but as the Deborah number increases the fraction of power dissipated by the polymers begins to grow and overwhelms the solvent dissipation for $De \lessapprox 1$. However, as the Deborah number is further increased, this trend is inverted and the fraction of power dissipated by the polymers decreases substantially, and by $De \approx 7$ most of the power input is again dissipated by the solvent $\varepsilon^{[s]} > \varepsilon^{[p]}$.

This complex behaviour of the solvent and polymer dissipations with the Deborah number, already observed in Valente *et al.*,[15] but here confirmed for a wider range of high Deborah numbers, is consistent with the competing effects of the relaxation time on the polymer dissipation. Indeed, on the one hand the polymer dissipation is inversely proportional to the relaxation time since $\varepsilon^{[p]} \equiv \left\langle f(C_{ii})\sigma^{[p]}_{jj} \right\rangle / 2\tau$, but on the other hand the polymer dissipation is also proportional to the mean square polymer extension, which increases monotonically with the polymer relaxation time (this can be inferred from Table I). Therefore, the decrease in the polymer dissipation beyond $De = O(1)$ indicates a weaker increase of the mean square polymer extension for larger polymer relaxation times. This is perhaps not surprising as the fluid is subjected to both viscous stress which react instantly to changes in the rate of deformation and elastic stresses which built up over time (and thus not instantaneously). Therefore, for turbulent fluid motions that are fast compared to the relaxation time (i.e., large Deborah numbers), the build-up of elastic stresses is not as efficient.

Figure 1(b) shows the normalised solvent dissipation, $C_{\varepsilon^{[s]}} \equiv (3/2)^{5/2}\varepsilon^{[s]}\ell/K^{3/2}$ and the normalised total power dissipated $C_P \equiv (3/2)^{5/2} P\,\ell/K^{3/2}$, as a function of the Deborah number (the numerical factor $(3/2)^{5/2}$ is used to allow a direct comparison with experimentally measured isotropic surrogates). The non-dimensional parameter C_P can be thought of as a measure of the efficiency of the flow to dissipate the external energy input at the large scales. Similar to the observation that the polymer dissipation was largest for $De = O(1)$, the numerical value of C_P also reaches a maximum for these Deborah numbers. However, for larger Deborah numbers C_P decreases and appears to tend towards the normalised solvent dissipation $C_{\varepsilon^{[s]}}$.

One may be misled to think that the decrease in the polymer dissipation for large Deborah numbers ($De > 1$) is a symptom of a decreasing effect of the polymers on the non-linear energy cascade dynamics, owing to the increasing gap between the characteristic turbulence/fluid time scales. However, this is not the case as discussed below.

Figure 2(a) shows the terms in Eq. (8) normalised with the total power input ($P = \sum_k f(k)$) for simulation #15 (see Table I). A similar wavenumber budget is observed for the other high Deborah number simulations.[15] It is clearly noticeable that $\Pi(k)$, which represents the kinetic energy flux associated with the non-linear energy cascade, is very small compared to the other energy exchanges in play.

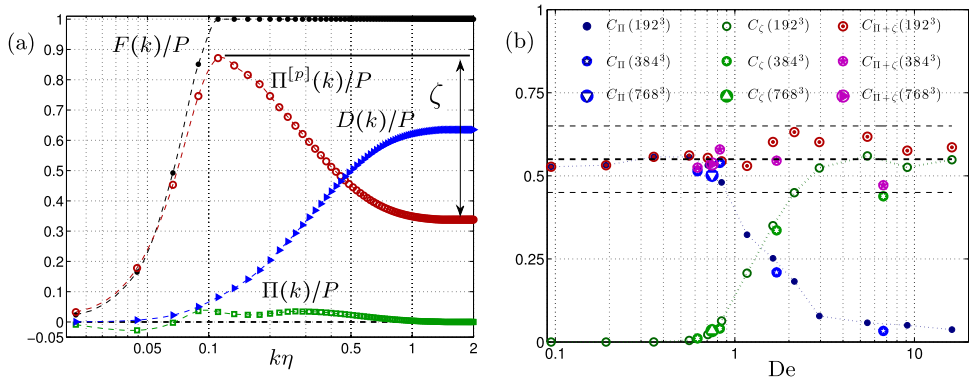

FIG. 2. (a) Terms of the wavenumber-by-wavenumber kinetic energy transfer budget (Eq. (8)) for the largest Deborah number dataset ($De = 16.2$, set # 15 in Table I). The polymer induced kinetic energy flux injected in the large wavenumbers, ζ, is illustrated in the figure. (b) Normalised maximum non-linear energy cascade flux, $C_\Pi \equiv (3/2)^{5/2}\Pi|_{\max}\ell/K^{3/2}$, normalised polymer induced kinetic energy cascade flux, $C_\zeta \equiv (3/2)^{5/2}\zeta\ell/K^{3/2}$, and normalised total kinetic energy cascade flux, $C_{\Pi+\zeta} \equiv (3/2)^{5/2}(\Pi|_{\max}+\zeta)\ell/K^{3/2}$ versus the Deborah number.

Reuse of AIP Publishing content is subject to the terms at: https://publishing.aip.org/authors/rights-and-permissions. Downloaded to IP: 193.136.33.229 On: Fri, 22 Jul 2016 15:24:55

In contrast $\Pi^{[p]}(k)$, which represents the kinetic to elastic energy transfer, plays a dominant role in the energy dynamics. The kinetic energy dissipated by the polymers (which is on average equal to the polymer dissipation due to the statistical stationarity) is $\varepsilon^{[p]} = \left\langle \sigma_{ij}^{[p]} S_{ij} \right\rangle = \Pi^{[p]}(k_{\max})$, where $k_{\max}$ is the maximum wavenumber. Since $\Pi^{[p]}(k)$ is maximum at some intermediate wavenumber k and decreases after this up to the maximum wavenumber $k_{\max}$, this indicates that more kinetic energy is removed from the large scales and converted to elastic energy than that dissipated by the polymers, and the additional power is returned back to the solvent at high wavenumbers. This is effectively a polymer induced kinetic energy cascade, i.e., a different "nature" of energy cascade prompted by the complex interplay between solvent and polymer molecules, which is not present for smaller values of De, as discussed in Valente *et al.*[15] The parameter $\zeta \equiv \max[\Pi^{[p]}(k)] - \Pi^{[p]}(k_{\max})$, introduced in Valente *et al.*[15] to quantify this polymer induced kinetic energy cascade flux, is also illustrated in Fig. 2(a). The present results carried out at much higher Deborah numbers clearly confirm the dominant role played by the polymers on the turbulence dynamics at high Deborah numbers.

The dimensionless parameters $C_\Pi \equiv (3/2)^{5/2}(\Pi_{\max})\,\ell/K^{3/2}$, $C_\zeta \equiv (3/2)^{5/2}(\zeta)\,\ell/K^{3/2}$, and $C_{\Pi+\zeta} \equiv (3/2)^{5/2}(\Pi_{\max}+\zeta)\,\ell/K^{3/2}$, representing the efficiency of the flow to cope with the energy flux from the large scales, were studied in Valente *et al.*[15] for Deborah numbers up to $De \approx 2$, where it was observed that $C_{\Pi+\zeta} \approx 0.5$, which is similar to the numerical value of C_Π for statistically steady[15,39,40] and unsteady (e.g., decaying) turbulence.[41,42] In the present work we extend this computation to the range of available Deborah numbers (up to $De \approx 10$), and the results are displayed in Fig. 2(b). Remarkably, our data show that this same numerical value persists for higher De numbers where the non-linear energy cascade is residual, i.e., $C_{\Pi+\zeta} \approx C_\zeta \approx 0.5$ and $C_\Pi \to 0$, cf. Fig. 2(b). Thus, the sum of the maximum non-linear energy cascade flux, $\Pi|_{\max}$ ($\equiv \max[\Pi(k)]$), with the polymer induced kinetic energy cascade flux, ζ, follows approximately the same fraction of the kinetic energy over the turnover time as the usual energy cascade flux in Newtonian turbulence.

This is a non-trivial result since the numerical value of $C_{\varepsilon^{[s]}}$ cannot be mathematically bounded as it was rigorously demonstrated for Newtonian turbulence using the functional shape of the body force.[43] This is owed to the fact that for polymer-laden turbulence there are two dissipation routes for the injected power. As can be appreciated in Fig. 1(b), the normalised power-input C_P takes very different numerical values throughout the range of Deborah numbers assessed and differs drastically from the behaviour of $C_{\varepsilon^{[s]}}$ and $C_{\Pi+\zeta}$.

The fact that a scaling which is characteristic of the classic non-linear kinetic energy cascade also holds when the polymers dominate the kinetic energy transfer suggests that the non-linear energy cascade may still play an important, although indirect, role. In order to investigate the decrease of the net non-linear energy cascade $\Pi(k)$ observed at high Deborah numbers, we compute its counterpart in the physical space.

Following a classical approach,[44] a (low pass) spatial filtering operation is used to separate any given flow variable $\phi(\vec{x},t)$ into large (or resolved) $\overline{\phi}(\vec{x},t;k_\Delta)$, and small (or residual) $\phi'(\vec{x},t;k_\Delta)$, components

$$\phi(\vec{x},t) = \overline{\phi}(\vec{x},t;k_\Delta) + \phi'(\vec{x},t;k_\Delta). \tag{9}$$

In the present work a sharp or cut-off filter, with filter width $k_\Delta = \pi/\Delta$, and defined by,

$$\widehat{G}_\Delta(\vec{k}) = \begin{cases} 1 & |\vec{k}| < k_\Delta \\ 0 & \text{otherwise} \end{cases},$$

is used to separate the large and small scales of motion, through the (spatial) filtering operation,

$$\overline{\phi}(\vec{x},t;k_\Delta) = FFT^{-1}\left\{\widehat{G}_\Delta(\vec{k})\widehat{\phi}(\vec{k},t)\right\}, \tag{10}$$

where FFT^{-1} represents the inverse Fourier transform.

The so-called subgrid-scale dissipation $\overline{\varepsilon}(\vec{x},t;k_\Delta) = -\tau_{ij}\overline{S_{ij}}$, where $\tau_{ij} = \overline{u_i u_j} - \overline{u_i}\,\overline{u_j}$ is the residual (or subgrid-scale) stresses tensor, represents the kinetic energy flux between large and small scales, separated at a given filter size Δ. $\overline{\varepsilon}(\vec{x},t;k_\Delta) > 0$ represents a local energy flux from large into small scales (direct cascade or forward scatter), whereas $\overline{\varepsilon}(\vec{x},t;k_\Delta) < 0$ represents an inverse energy flux (inverse cascade or "backscatter") from small into resolved scales.[40,44,45]

Reuse of AIP Publishing content is subject to the terms at: https://publishing.aip.org/authors/rights-and-permissions. Downloaded to IP: 193.136.33.229 On: Fri, 22 Jul 2016 15:24:55

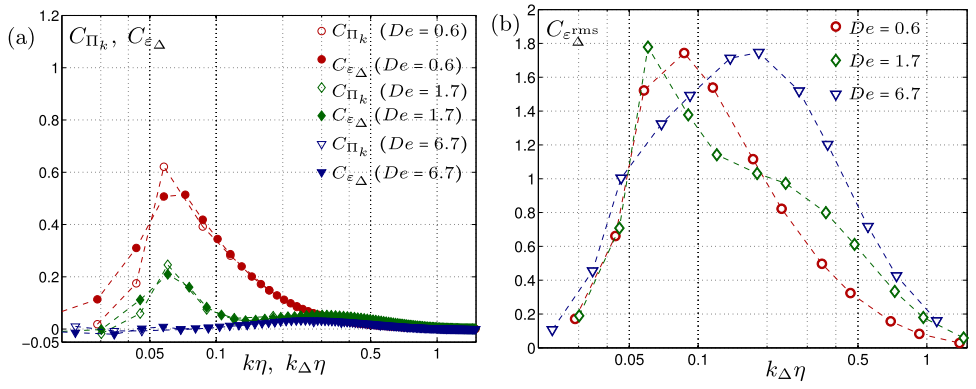

FIG. 3. (a) Normalised energy transfer flux $C_{\Pi_k} \equiv (3/2)^{5/2}\Pi(k)\ell/K^{3/2}$ and normalised mean subgrid-scale dissipation $C_{\varepsilon_\Delta} \equiv (3/2)^{5/2}\langle\overline{\varepsilon}(k_\Delta)\rangle\ell/K^{3/2}$ for several filter sizes $\Delta/\eta = \pi/(k_\Delta\eta)$ ($k_\Delta\eta$ is the normalised cut-off wave number), for several simulations with different Deborah numbers (see Table I); (b) normalised root mean square of the subgrid-scale dissipation, $C_{\varepsilon_\Delta^{\rm rms}} \equiv (3/2)^{5/2}\overline{\varepsilon}^{\rm rms}(k_\Delta)\ell/K^{3/2}$, where $\overline{\varepsilon}^{\rm rms}(k_\Delta)$ is the root mean square of the subgrid-scale dissipation for filter size $k_\Delta = \pi/\Delta$.

Figure 3(a) shows a comparison between the normalised non-linear energy cascade flux $C_{\Pi_k} \equiv (3/2)^{5/2}\Pi(k)\ell/K^{3/2}$ and $C_{\varepsilon_\Delta} \equiv (3/2)^{5/2}\langle\overline{\varepsilon}(\vec{x},t;k_\Delta)\rangle\,\ell/K^{3/2}$, i.e., the normalised mean (volume-averaged) subgrid-scale dissipation at filter scale k_Δ.

One confirms that the mean subgrid-scale dissipation is a reasonable surrogate for the actual non-linear energy transfer, i.e., $\langle\overline{\varepsilon}\rangle(k_\Delta) \approx \Pi(k)$ (see Fig. 3(a)) and again one notices the depletion of the net non-linear energy flux to small scales for increasing Deborah numbers. However, this by no means implies that the local non-linear energy cascade is inactive. To show this, we plot in Fig. 3(b) the root mean square of the subgrid-scale dissipation, i.e., $\overline{\varepsilon}^{\rm rms} = \sqrt{\langle\overline{\varepsilon}^2\rangle - \langle\overline{\varepsilon}\rangle^2}$, for several filter sizes for three different Deborah numbers and in dimensionless form. As noted before, as *De* increases there is a monotonic decrease in the net non-linear energy cascade (Fig. 3(a)). However, the root mean square of the subgrid-scale dissipation, $\overline{\varepsilon}^{\rm rms}$, which is a measure of the activity of the non-linear energy transfers from triadic interactions,[40] does not concomitantly decrease with the net energy cascade (Fig. 3(b)). Instead, it seems to remain approximately proportional to the total energy cascade flux, $\Pi|_{\max} + \zeta$ and to $K^{3/2}/\ell$.

To explain this result the average normalised subgrid-scale dissipation, separated into forward cascade $\overline{\varepsilon}_+(\vec{x},t;k_\Delta) = \overline{\varepsilon}(\vec{x},t;k_\Delta)$ if $\overline{\varepsilon} > 0$ (and 0 otherwise) and backward energy cascade $\overline{\varepsilon}_-(\vec{x},t;k_\Delta) = \overline{\varepsilon}(\vec{x},t;k_\Delta)$ if $\overline{\varepsilon} < 0$ (and 0 otherwise) contributions, is shown in Fig. 4 as $C_{\varepsilon_\Delta^+} \equiv (3/2)^{5/2}$ $\langle\overline{\varepsilon}_+(\vec{x},t;k_\Delta)\rangle\,\ell/K^{3/2}$ and $C_{\varepsilon_\Delta^-} \equiv (3/2)^{5/2}\langle\overline{\varepsilon}_-(\vec{x},t;k_\Delta)\rangle\,\ell/K^{3/2}$, respectively. As the Deborah number

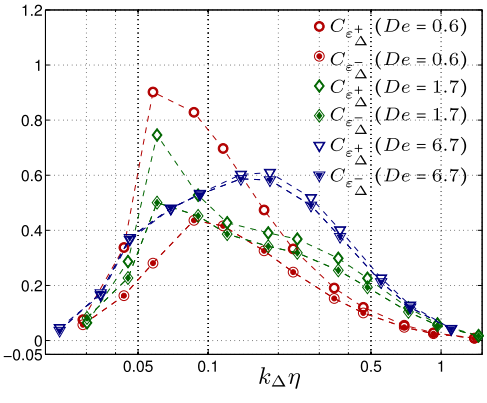

FIG. 4. Forward, $C_{\varepsilon_\Delta^+}$ and backward, $C_{\varepsilon_\Delta^-}$, energy fluxes to/from subgrid-scales normalised by the kinetic energy and eddy turnover time (see Fig. 3 for the analogous definitions of C_{ε_k} and C_{ε_Δ}), as a function of the filter size k_Δ showing both an increase in the normalised backward energy flux ("backscatter") and a decrease in the forward normalised energy flux for increasing Deborah numbers, both contributing to the depletion of the net energy flux shown in Fig. 3(a).

Reuse of AIP Publishing content is subject to the terms at: https://publishing.aip.org/authors/rights-and-permissions. Downloaded to IP: 193.136.33.229 On: Fri, 22 Jul 2016 15:24:55

increases one observes both a decrease of the forward energy cascade and an increase of the backward energy cascade resulting in an almost full depletion of the net non-linear energy cascade for $De = 6.7$. These are interesting results illustrating that the non-linear energy exchanges can play an important role even when the net non-linear energy cascade is negligible.

It may be the case that the kinetic energy re-injected by the polymers at large wavenumbers (ζ) is indirectly set by these non-linear energy exchanges, which would be consistent with the fact that for very large De, $\Pi|_{\max} \approx 0$ and ζ remains approximately the same fraction of the kinetic energy over the turnover time as the energy cascade in Newtonian turbulence, i.e., $C_\zeta \approx 0.5$. However, for the time being, this is no more than a conjecture for which we have no proof and that requires further investigation. Nevertheless, if this is the case, it is unlikely that this scaling behaviour persists for very low Reynolds numbers in the elastic turbulence regime.[46]

B. Consequences for the energy spectra

We now turn the attention to the shape of the kinetic energy spectrum for the range of De covered by our data which supplements the available data from quasi-homogeneous turbulence experiments[18,47,48] and from periodic box turbulence DNSs,[17,38,49–51] with substantially larger Deborah numbers.

For moderately low De, the available data consistently indicate a steepening of the kinetic energy spectra beyond a wavenumber, k_L, which is often associated with Lumley's length-scale.[18,30,49] In some cases, the steepening of the energy spectra is interpreted as the onset of the steeper power-law range, k^χ, with $\chi \approx -3$ (Ref. 18 and references therein) or $\chi \leq -3$ (Refs. 3 and 16) predicted by theoretical arguments. In this scenario, the inertial range of polymer laden turbulence would consist of a $k^{-5/3}$ inertial sub-range up to Lumley's wavenumber k_L and a k^χ range for larger wavenumbers. Recall that in Newtonian turbulence, the inertial range consists of scales which are too large to be affected by viscosity and too small to be affected by the external power input or large-scale inhomogeneities. However, since the polymers can affect the inertial range of scales, in particular below k_L, we denote this region as the elasto-inertial range.[8] Owing to the limited Reynolds numbers straddled by the existing experiments and simulations there is little evidence clearly supporting the co-existence of the two power-laws, i.e., $\sim k^{-5/3}$ followed by a steeper power-law, perhaps with the sole exception being the recent laboratory data presented by Vonlanthen and Monkewitz.[18] This is also the case for our limited Reynolds number data, where it can be seen that the elasto-inertial range of the spectra appears to reach slopes steeper than $\chi = -5/3$ as De is increased up to $De \approx 0.8$, but it is difficult to identify a $k^{-5/3}$ inertial sub-range preceding these steeper power-laws (see Fig. 5; note that only our data with $N = 192^3$ collocation points, including the data with hyperviscosity, cover this low De regime). Also in agreement with previous authors (see Vonlanthen and Monkewitz[18] and references therein), we only observe a steepening of the spectra above the wavenumber corresponding to Lumley's scale (Fig. 5). We note that, regardless of the existence of a steeper power-law range for length-scales below the Lumley scale and within the elasto-inertial range, the reduction of spectra energy density at large wavenumbers is a direct consequence of the decrease of the solvent dissipation, $\varepsilon^{[s]}$, which only occurs for low to moderate Deborah numbers (see Fig. 1(a); recall that $\varepsilon^{[s]} = 2\nu^{[s]} \sum_k k^2 E(k)$).

For large De, this decreasing trend in the solvent dissipation is reversed (beyond $De \approx 0.8$ according to our data, see Fig. 1(a)) and consequently there is a concomitant augmentation of the kinetic energy of the small scales (see Fig. 6). More importantly, the slope of the power-law region becomes shallower and seems to tend towards $k^{-5/3}$ (see Figs. 5(b)–5(d) and 7(b)). This is surprising because for large De the non-linear energy cascade is effectively negligible (cf. Fig. 2(b)). In Fig. 7(a) we compensate the spectra by $k^{-5/3}$ but normalise it using the total energy flux to the small scales, $\Pi_{\max} + \zeta$ and the integral-scale. Remarkably, our data seem to support the possibility that the functional form of the elasto-inertial power-law range for large Re_λ and De numbers is $E(k) \sim (\Pi_{\max} + \zeta)^{2/3} k^{-5/3}$. Nevertheless, the data obtained using $N = 192^3$ collocation points straddle too low Re_λ to obtain a plausible inertial range. Interestingly, for low De, the same functional form may hold, but since $\zeta = 0$ and $\Pi_{\max} = \varepsilon^{[s]}$ (at least if the flow is statistically steady, see discussion in Valente *et al.*[15]) it reverts to

Reuse of AIP Publishing content is subject to the terms at: https://publishing.aip.org/authors/rights-and-permissions. Downloaded to IP: 193.136.33.229 On: Fri, 22 Jul 2016 15:24:55

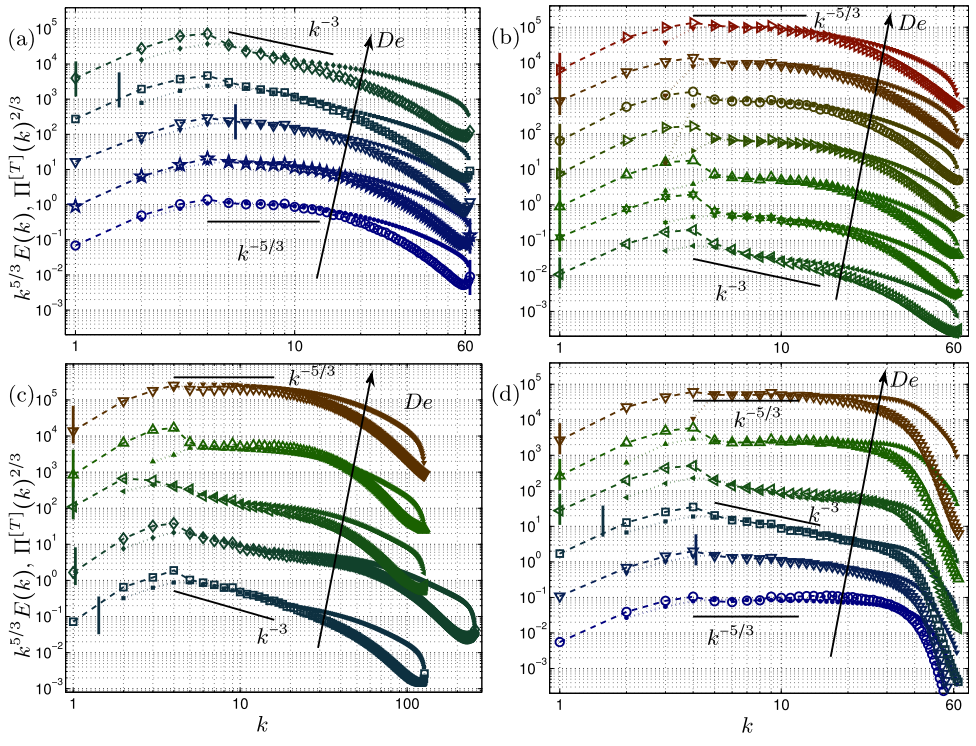

FIG. 5. Compensated kinetic energy spectra, $k^{5/3}E(k)$ (large open symbols) compared with the two-thirds power of the total kinetic energy cascade flux spectra, $\Pi^{[T]}(k)^{2/3}$ (small filled symbols) for the viscoelastic DNSs with (a) $N = 192^3$ and $0.1 \le De \le 0.71$, (b) $N = 192^3$ and $0.71 \le De \le 16.2$, (c) $N = 384^3$ and $N = 768^3$ (distinguishable by the maximum wavenumber value) and $0.62 \le De \le 6.7$ and (d) $N = 192^3$, $0.1 \le De \le 7.1$ with hyper-viscous dissipation (see Table I). The total energy cascade flux spectrum $\Pi^{[T]}(k)$ is defined in Eq. (12) and quantifies the total downscale kinetic energy flux provided by the usual non-linear energy cascade together with the polymer induced kinetic energy cascade. The spectra $\Pi^{[T]}(k)^{2/3}$ are multiplied by an arbitrary factor such that it overlaps $k^{5/3}E(k)$ within a power-law region (typically $5 \le k \le 10$). The results for each DNS are offset by another arbitrary factor such that the various spectra are distinguishable. The wavenumber corresponding to the Lumley scale, k_L, is represented with a vertical solid line (whenever k_L is smaller/larger than $k_{\min}/k_{\max}$, it is set to $k_{\min}$ or $k_{\max}$, respectively). Reference power-laws with $-5/3$ and -3 are plotted with solid black lines.

the celebrated Kolmogorov-Obukhov spectrum for Newtonian turbulence,[34] $E(k) \sim \varepsilon^{2/3}k^{-5/3}$. This is also illustrated in Fig. 7(a), albeit for low Re_λ data only.

It should be noted that $E(k) \sim (\Pi_{\max} + \zeta)^{2/3}k^{-5/3}$ is consistent with the fact that the low wavenumber part of the spectra scales with ℓ and K (Fig. 6) together with the fact that $(\Pi_{\max} + \zeta) \sim K^{3/2}/\ell$ (Fig. 2(b)), since $E(k) \sim (\Pi_{\max} + \zeta)^{2/3}k^{-5/3}$ can be re-written as $E(k)/(K\ell) \sim C_{\Pi+\zeta}^{2/3}(k\ell)^{-5/3}$. Remarkably, the fact that $C_{\Pi+\zeta}$ also appears to be constant and independent of the Deborah number implies that both the low and the large Deborah number spectra collapse in this power-law range.

In what follows we suggest an interpretation for the change of the power-law slope of the energy spectra. We employ classical dimensional arguments in order to relate the slopes of the power-law regions of $E(k)$ and $\Pi(k)$ and provide further data illustrating how the kinetic to elastic energy flux spectra $\Pi^{[p]}(k)$ influence the functional form of the energy cascade flux $\Pi(k)$, which in turn influence the shape of the kinetic energy spectra $E(k)$. Within Kolmogorov's phenomenology, the inertial-range energy spectrum is solely a function of k and ε (= $\Pi(k)$ for these wavenumbers), which leads to the Kolmogorov-Obukhov spectrum,[34] $E(k) \sim \varepsilon^{2/3}k^{-5/3}$. Building upon Kolmogorov's theory, many general models were suggested for determining $\Pi(k)$ from integro-differential equations of $E(k)$ (see Sec. 17 in Ref. 52). Regardless of the particular choice of model, $E(k) \sim k^{-5/3}$ always leads to $\Pi(k) \sim$ constant (i.e., a plateau of constant flux) and vice versa. Note, however, that these models relate the functional forms of $E(k)$ and $\Pi(k)$, but obviously require the knowledge of one of them. In Kolmogorov's framework this is achieved by postulating that the inertial-range flux is constant and equal to the dissipation due to local equilibrium, $\Pi(k) = \varepsilon$ (this is

Reuse of AIP Publishing content is subject to the terms at: https://publishing.aip.org/authors/rights-and-permissions. Downloaded to IP: 193.136.33.229 On: Fri, 22 Jul 2016 15:24:55

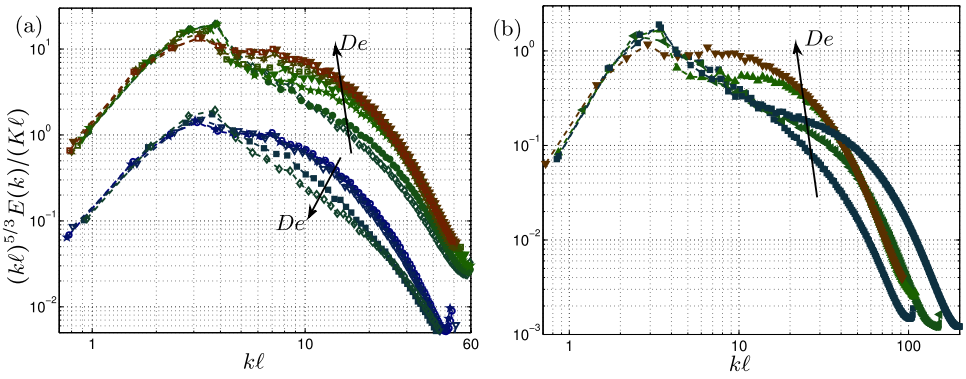

FIG. 6. Compensated kinetic energy spectra normalised with large scale variables, K and ℓ, for the various viscoelastic DNSs with (a) $N = 192^3$ (excluding DNSs with hyperviscosity) and (b) $N = 384^3$ or $N = 768^3$ collocation points (see Table I). The slope of the power-law region in figure (a) exhibits two distinct trends with the Deborah number and thus are grouped for convenience. For the lower group, which corresponds to a lower Deborah number range, $0.1 \le De \le 0.71$, the slope of the power law region increases with the Deborah number. For larger Deborah numbers, $0.71 \le De \le 16.2$, the trend is reversed and slope becomes progressively shallower and tends towards $k^{-5/3}$ (this group of spectra is vertically offset by a factor of 10; note that the data for the highest De of the lower group represented with empty diamonds are also included in the upper group). In figure (b) the steepest spectra correspond to $De \approx 0.6$, and for larger De the slope of the power-law range also becomes shallower and appears to tend towards $-5/3$.

usually known in its isotropic form as Kolmogorov's four-fifths law). For polymer-laden turbulence the elasto-inertial range can be affected by the polymers and therefore $\Pi(k) \sim$ constant will not hold in general. Instead, let us postulate that for scales within this elasto-inertial range the spectra follow the power-laws $\Pi(k) \sim k^{\gamma}$ and $E(k) \sim k^{\chi}$. For any model relating $\Pi(k)$ with $E(k)$ and k, these exponents are closely related due to dimensional constraints by

$$\frac{2}{3}\gamma = \frac{5}{3} + \chi \tag{11}$$

(cf. Eq. 17.19 in Ref. 52). The same relation can be derived from the recent result presented in Ref. 53.

We tested this idea against our DNS data and found that it seems consistent with our data as long as the polymers remove energy from all the scales, i.e., $\zeta \approx 0$ (see Fig. 5(a) and note that

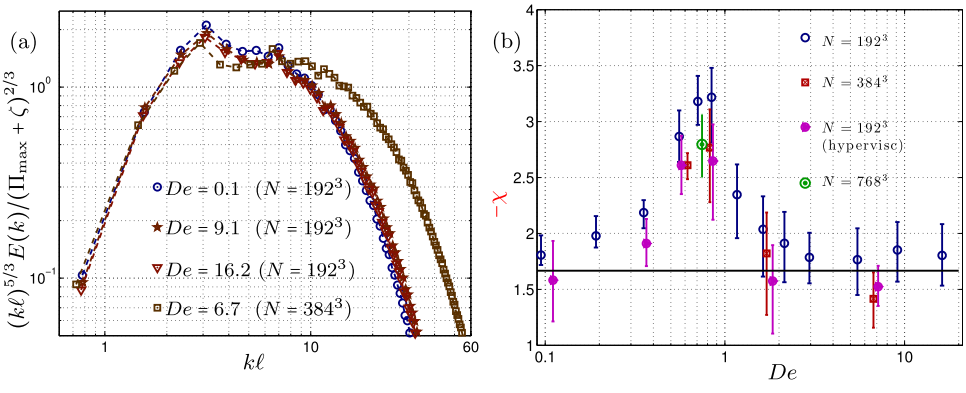

FIG. 7. (a) Compensated kinetic energy spectra normalised with the total kinetic energy cascade flux, $\Pi_{max}+\zeta$ and ℓ, for one low and three high De number DNSs, suggesting that $E(k) \sim (\Pi_{max}+\zeta)^{2/3}k^{-5/3}$ may be a good approximation to the functional form for the elasto-inertial range of scales (note that for low De, $\zeta \approx 0$ and the proposed functional form reverts to the Kolmogorov-Obukhov spectrum). (b) Slope χ of the power-law k^{χ} (multiplied by -1) fitted to the elasto-inertial range of scales for various De, showing that the steeper power-laws only occur for intermediate Deborah numbers of order unity (all the datasets shown in Table I are presented). The error bars represent three similar fits applied to different ranges of wavenumbers.

Reuse of AIP Publishing content is subject to the terms at: https://publishing.aip.org/authors/rights-and-permissions. Downloaded to IP: 193.136.33.229 On: Fri, 22 Jul 2016 15:24:55

for these low De, $\Pi^{[T]}(k) \approx \Pi(k)$, where $\Pi^{[T]}(k)$ is the total kinetic energy cascade flux spectrum defined below). When the polymers re-inject energy into the small scales, this is effectively a kinetic energy cascade that is complementary to $\Pi(k)$. However, adding the two kinetic energy cascade fluxes is not straightforward since $\Pi^{[p]}(k)$ includes both the flux of kinetic energy extracted from the solvent and dissipated by the polymers and the flux of kinetic energy transferred/cascaded by the polymer to small solvent scales. To overcome this difficulty we propose a simple, but non-unique, definition for the total kinetic energy cascade flux spectrum,

$$\Pi^{[T]}(k) \equiv \begin{cases} \Pi(k) + \left(\Pi^{[p]}(k) - \Pi^{[p]}(k_{\max})\right) & \forall k : \left(\Pi^{[p]}(k) - \Pi^{[p]}(k_{\max})\right) \geq 0 \\ \Pi(k) & \text{otherwise} \end{cases}. \tag{12}$$

Although this definition is non-unique, it satisfies the requisite for an inter-scale transfer flux $\Pi^{[T]}(k_{\min}) = \Pi^{[T]}(k_{\max}) = 0$. Other definitions could be sought for this total flux, but any definition leading to $\Pi^{[T]}(k_{\max}) = 0$ leads to the same functional form for $\Pi^{[T]}$ beyond the wavenumber $k = k_\star$, where $k_\star$ is the wavenumber where $\Pi^{[T]}$ is maximal, which turns out to be the range of wavenumbers where the power-law behaviour of $\Pi^{[T]}$ occurs (see Fig. 5).

Having defined a total kinetic energy flux, we may now re-assess the adequateness of Eq. (11) applied to the relationship between the power-laws $\Pi^{[T]}(k) \sim k^\gamma$ and $E(k) \sim k^\chi$. Indeed our data support that there is a range of scales exhibiting power-law slopes compatible with the constraint posed by Eq. (11) (see Fig. 5). This is particularly visible in the hyperviscous FENE-P DNSs which have a broader elasto-inertial range (Fig. 5(d)).

Thus far we showed how both the steepening of the kinetic energy spectrum for low to moderate De and the tendency for recovering the $k^{-5/3}$ for large De may be related to the change in the power-law slope of the total cascade flux $\Pi^{[T]}(k)$. We now investigate the dynamics leading to the various slopes of $\Pi^{[T]}(k)$. We start by noting that in homogeneous statistically steady viscoelastic turbulence, the elasto-inertial range is characterised by $f(k) \approx 0$, $2\nu k^2 E(k) \approx 0$ and thus $T(k) \approx T^{[p]}$ (cf. Eq. (7)). As noted above, if the sign of $T^{[p]}$ is such that the net effect at every wavenumber within this range is to remove kinetic energy from the solvent, this energy can only be supplied via non-linear interactions and thus $T(k) \approx T^{[p]} \neq 0$. This occurs at low to moderate De where the polymer induced energy cascade is negligible (the polymers act mostly as an energy sink for all wavenumbers) and thus $\Pi^{[T]}(k) \approx \Pi(k)$. In this scenario, $T(k) > 0$ (since the non-linear interactions are supplying energy) and $\Pi(k)$ will have a negative slope ($\gamma < 0$) leading to the steepening of the kinetic energy spectrum ($\chi < -5/3$ according to Eq. (7)). Conversely, if $T^{[p]}$ has the tendency to re-inject energy at large wavenumbers, it cannot do so within this elasto-inertial range unless it would drive an upscale non-linear cascade within this elasto-inertial range. In practice it does not appear to happen and thus $T^{[p]} \approx T(k) \approx 0$, leading to $\Pi^{[T]}(k) \sim k^0$, which is just like Newtonian turbulence where $T(k) \approx 0$ and $\Pi(k) \sim$ constant which may explain why the $k^{-5/3}$ power-law is recovered. As noted before, the inertial range flux is roughly $\Pi|_{\max} + \zeta$ leading to the functional form, $E(k) \sim (\Pi_{\max} + \zeta)^{2/3} k^{-5/3}$, which is compatible with our data (Fig. 7(a)).

We note in passing that the various forms of the spectrum are discussed here within the context of our statistically steady state viscoelastic turbulence simulations. For the more general case of transient or unsteady turbulence the functional form of the spectrum may also depend on the time-derivative of the dissipation and/or the energy cascade flux leading to transient parts of the spectra with $-7/3$ or $-9/3$ slopes.[54,55]

A final remark concerns the effect of the viscosities ratio, β. Valente *et al.*[15] analysed the effects in the ranges $0.8 \leq \beta \leq 0.95$ and $0 \leq De \leq 2$ and showed that for $De \leq 0.2$, when polymer molecules are weakly stretched, the fractions of solvent and polymer dissipations (of the total dissipation) are directly proportional to β and $(1 - \beta)$, respectively. As De increases polymers stretch and participate more actively in the turbulence dynamics, dissipating an increasingly larger fraction of the power input, but with the effect of β decreasing significantly so that only a mild dependence on β is registered. This is related to the fact that the polymer stresses vary directly with the $(1 - \beta)$ and polymer stretch, but the latter is inversely proportional to $(1 - \beta)$, so that there is some compensation which is consistent with arguments put forward by Balbovsky *et al.*[3] Hence, it

Reuse of AIP Publishing content is subject to the terms at: https://publishing.aip.org/authors/rights-and-permissions. Downloaded to IP: 193.136.33.229 On: Fri, 22 Jul 2016 15:24:55

is not expected that variations in β will change significantly the above reported variations in energy spectra and only minor quantitative variations are expected.

IV. CONCLUSIONS

We present new DNSs of statistically stationary periodic box turbulence of FENE-P fluids for large Deborah numbers ($De > 1$) and investigate this inertio-elastic regime where the polymers become less relevant as a kinetic energy dissipator (contrary to the case for moderate De) but play an increasingly important role in transferring kinetic energy from large to small scales effectively replacing the usual non-linear energy cascade mechanism which, in turn, becomes negligible. We show that the strong reduction of the net non-linear energy cascade is due to the fact that the energy exchanges from small to large scales (reverse cascade or "backscatter") increase and nearly balance the energy exchanges from large to small scales (the usual forward cascade which is also reduced as De increases). This strongly indicates that non-linear energy exchanges are highly active even when they virtually do not transfer kinetic energy to small scales. This may tentatively explain why the overall kinetic energy cascade is still proportional to the kinetic energy over the turnover time, just like for turbulence in Newtonian fluids.

We further show that the previously observed steepening of the kinetic energy spectrum only occurs for low to moderate Deborah numbers and that for large Deborah numbers it seems to revert to a $k^{-5/3}$ power-law for a range of wavenumbers where there is no power added by the forcing nor removed by viscous (solvent) dissipation, i.e., an inertio-elastic range where inertia and elasticity are dominant. In this range the spectra appear to scale with the total kinetic energy flux to the small scales leading to a new functional form $E(k) \sim (\Pi_{\max} + \zeta)^{2/3} k^{-5/3}$ which can be thought of as an extension of the usual Kolmogorov-Obukhov power-law for inertio-elastic turbulence.

Nevertheless, we stress that our DNS data only straddle moderately low Reynolds numbers preventing clear power-law ranges to be obtained. Although our conclusions are supported by the hyperviscous simulations, this is only a qualitative indication of what may happen for the inertio-elastic range at larger Re_λ. Furthermore, the adequacy of the FENE-P model as a rheological model for strong polymer-turbulence interactions remains to be fully assessed; a preliminary investigation on the use of the FENE-P as an approximation for the FENE dumbbell by Zhou and Akhavan[56] is restricted to turbulent channel flow at low Reynolds number. Reassuringly, we have used large maximum polymer extensibilities such that the model behaves quasi-linearly, but the FENE-P equation is a poor approximation of the FENE dumbbell especially in transient flows[57] and especially if they have an extensional nature as happens locally in vortex stretching events. The FENE equation is a kinetic theory type constitutive equation describing the flow-induced configuration of polymers in dilute solutions using a coarse-grained approach. It exhibits an hysteretic behavior in the stress response to molecular extension when subject to cycles of extension and relaxation as found also experimentally,[58,59] which is absent from the FENE-P closure. Unfortunately, the large number of degrees of freedom of the configuration space does not allow for an equivalent macroscopic closure to be developed and the direct use of the FENE dumbbell in DNS of turbulent flows is still prohibitively expensive, and the more so of a more realistic multibead FENE equation. Therefore, this type of simulations relies on models based on restrictions of the configuration space of the FENE dumbbell, such as the FENE-P for which there is today a large body of literature, taking into account only the longest relaxation time of the polymers. Other closures of the FENE equation containing an hysteretic behavior do exist, such as the FENE-L,[60] but these also have other limitations that need to be better assessed and in any case a spectrum of relaxation times is also needed that only a multimode model can capture. Indeed, at large De the shorter time scales of the polymer chains may also play an important role in the physics which the current simulations cannot investigate and which are too expensive to be performed using a multibead FENE model. In Sec. III we suggest experiments which could, in principle, investigate the current inertio-elastic regime with state-of-the-art apparatuses. We believe that it would be highly valuable to obtain such data and further investigate this inertio-elastic regime in quasi-homogeneous turbulence.

Reuse of AIP Publishing content is subject to the terms at: https://publishing.aip.org/authors/rights-and-permissions. Downloaded to IP: 193.136.33.229 On: Fri, 22 Jul 2016 15:24:55

Finally we note that the present results illustrate the extraordinary behaviour of turbulence when additional degrees of freedom are present. The kinetic energy that the polymers inject into the small scales may share similarities with turbulent flows with living organisms, active scalars, and inertial particles, to name but a few examples. The well defined scaling behaviours exhibited for the inertio-elastic regime also bring optimism in developing turbulence models using the same tools and methodologies employed for turbulence in Newtonian fluids.

ACKNOWLEDGMENTS

The authors acknowledge the funding from COMPETE, FEDER, and Fundação para a Ciência e a Tecnologia (Grant No. PTDC/EME-MFE/113589/2009), and through IDMEC, under LAETA, Project Nos. PTDC/EME-MFE/122849/2010 and UID/EMS/50022/2013. The authors acknowledge the Laboratory for Advanced Computing at University of Coimbra (URL: http://www.lca.uc.pt) for providing HPC, computing and consulting resources that have contributed to the research results reported within this paper.

[1] J. L. Lumley, "Drag reduction in turbulent flow by polymer additives," J. Polym. Sci. **7**, 263–290 (1973).
[2] C. White and M. Mungal, "Mechanics and prediction of turbulent drag reduction with polymer additives," Annu. Rev. Fluid Mech. **40**, 235–256 (2008).
[3] E. Balbovsky, A. Fouxon, and V. Lebedev, "Turbulence of polymer solutions," Phys. Rev. E **64**, 056301 (2001).
[4] J. L. Lumley, "Drag reduction by additives," Annu. Rev. Fluid Mech. **1**, 367–384 (1969).
[5] I. Procaccia, V. S. L'Vov, and R. Benzi, "Colloquium: Theory of drag reduction by polymers in wall-bounded turbulence," Rev. Mod. Phys. **80**, 225–247 (2008).
[6] F.-C. Li and Y. Kawaguchi, "Investigation on the characteristics of turbulence transport for momentum and heat in a drag-reducing surfactant solution flow," Phys. Fluids **16**, 3281 (2004).
[7] V. Dallas, J. C. Vassilicos, and G. Hewitt, "Strong polymer-turbulence interactions in viscoelastic turbulent channel flow," Phys. Rev. E **82**, 066303 (2010).
[8] D. Samanta, Y. Dubief, M. Holzner, C. Schäfer, A. N. Morozov, C. Wagner, and B. Hof, "Elasto-inertial turbulence," Proc. Natl. Acad. Sci. U. S. A. **110**, 10557–10562 (2013).
[9] Y. Dubief, V. Terrapon, and J. Soria, "On the mechanism of elasto-inertial turbulence," Phys. Fluids **25**, 110817 (2013).
[10] R. Benzi, E. Ching, and E. de Angelis, "Effect of polymer additives on heat transport in turbulent thermal convection," Phys. Rev. Lett. **104**, 024502 (2010).
[11] F. De Lillo, G. Boffetta, and S. Musacchio, "Control of particle clustering in turbulence by polymer additives," Phys. Rev. E **85**, 036308 (2012).
[12] G. Boffetta, A. Mazzino, S. Musacchio, and L. Vozella, "Polymer heat transport enhancement in thermal convection: The case of Rayleigh-Taylor turbulence," Phys. Rev. Lett. **104**, 184501 (2010).
[13] L. Thais, A. E. Tejada-Martínez, T. B. Gatski, and G. Mompean, "Temporal large eddy simulations of turbulent viscoelastic drag reduction flows," Phys. Fluids **22**, 013103 (2010).
[14] L. Thais, T. B. Gatski, and G. Mompean, "Some dynamical features of the turbulent flow of a viscoelastic fluid for reduced drag," J. Turbl. **13**, N19, 1–26 (2012).
[15] P. C. Valente, C. da Silva, and F. Pinho, "The effect of viscoelasticity on the turbulent kinetic energy cascade," J. Fluid Mech. **760**, 39–62 (2014).
[16] A. Fouxon and V. Lebedev, "Spectra of turbulence in dilute polymer solution," Phys. Fluids **15**, 2060 (2003).
[17] P. Perlekar, D. Mitra, and R. Pandit, "Direct numerical simulations of statistically steady, homogeneous, isotropic fluid turbulence with polymer additives," Phys. Rev. E **82**, 066313 (2010).
[18] R. Vonlanthen and P. A. Monkewitz, "Grid turbulence in dilute polymer solutions: PEO in water," J. Fluid Mech. **730**, 76–98 (2013).
[19] R. Bird, C. Curtiss, R. Armstrong, and O. Hassager, *Dynamics of Polymeric Liquids*, 2nd ed. (John Wiley, New York, 1987), Vol. II.
[20] S. Jin and L. Collins, "Dynamics of dissolved polymer chains in isotropic turbulence," New J. Phys. **9**, 360 (2007).
[21] T. Vaithianathan, A. Robert, J. G. Brasseur, and L. Collins, "An improved algorithm for simulating three-dimensional, viscoelastic turbulence," J. Non-Newtonian Fluid Mech. **140**, 3–22 (2006).
[22] K. Alvelius, "Random forcing of three-dimensional homogeneous turbulence," Phys. Fluids **11**, 1880 (1999).
[23] V. Borue and S. A. Orszag, "Forced three-dimensional homogeneous turbulence with hyperviscosity," Europhys. Lett. **29**, 687–692 (1995).
[24] V. Borue and S. A. Orszag, "Numerical study of three-dimensional Kolmogorov flow at high Reynolds numbers," J. Fluid Mech. **306**, 293–323 (1996).
[25] V. Borue and S. A. Orszag, "Local energy flux and subgrid-scale statistics in three-dimensional turbulence," J. Fluid Mech. **366**, 1–31 (1998).
[26] P. Bartello, O. Métais, and M. Lesieur, "Coherent structures in rotating three-dimensional turbulence," J. Fluid Mech. **273**, 1–29 (1994).
[27] L. Smith and F. Waleffe, "Generation of slow large scales in forced rotating stratified turbulence," J. Fluid Mech. **451**, 145–168 (2002).
[28] G. Brethouwer, P. Billiant, E. Lindborg, and J.-M. Chomaz, "Scaling analysis and simulation of strongly stratified turbulent flows," J. Fluid Mech. **585**, 342–368 (2007).

Reuse of AIP Publishing content is subject to the terms at: https://publishing.aip.org/authors/rights-and-permissions. Downloaded to IP: 193.136.33.229 On: Fri, 22 Jul 2016 15:24:55

[29] S. Kida, S. Yanase, and J. Mizushima, "Statistical properties of MHD turbulence and turbulent dynamo," Phys. Fluids A **3**, 457 (1991).
[30] E. de Angelis, C. M. Casciola, R. Benzi, and R. Piva, "Homogeneous isotropic turbulence in dilute polymers," J. Fluid Mech. **531**, 1–10 (2005).
[31] N. Ouellette, H. Xu, and E. Bodenschatz, "Bulk turbulence in dilute polymer solutions," J. Fluid Mech. **629**, 375–385 (2009).
[32] I. Teraoka, *Polymer Solutions: An Introduction to Physical Properties* (Wiley Interscience, New York, 2002).
[33] Y. Liu, Y. Jun, and V. Steinberg, "Concentration dependence of the longest relaxation times of dilute and semi-dilute polymer solutions," J. Rheol. **53**, 1069–1085 (2009).
[34] U. Frisch, *Turbulence: The Legacy of AN Kolmogorov* (Cambridge University Press, Cambridge, 1995).
[35] C. C. Lin, "Remarks on the spectrum of turbulence," in *Proceedings of Symposia in Applied Mathematics, Providence, USA, 2–4 August 1947* (American Mathematical Society, 1949), Vol. 1, pp. 81–86.
[36] J. G. Brasseur, A. Robert, L. Collins, and T. Vaithianathan, "Fundamental physics underlying polymer drag reduction, from homogeneous DNS turbulence with the FENE-P model," in 2nd International Symposium on Seawater Drag Reduction, Busan, South Korea, 23–26 May 2005.
[37] C. M. Casciola and E. de Angelis, "Energy transfer in turbulent polymer solutions," J. Fluid Mech. **581**, 419–436 (2007).
[38] W.-H. Cai, F.-C. Li, and H.-N. Zhang, "DNS study of decaying homogeneous isotropic turbulence with polymer additives," J. Fluid Mech. **665**, 334–356 (2010).
[39] T. Gotoh and T. Watanabe, "Statistics of transfer fluxes of the kinetic energy and scalar variance," J. Turbul. **6**, N33 (2005).
[40] T. Ishihara, T. Gotoh, and Y. Kaneda, "Study of High-Reynolds number isotropic turbulence by direct numerical simulation," Annu. Rev. Fluid Mech. **41**, 165–180 (2009).
[41] W. D. McComb, A. Berera, M. Salewski, and S. Yoffe, "Taylor's (1935) dissipation surrogate reinterpreted," Phys. Fluids **22**, 061704 (2010).
[42] P. C. Valente, R. Onishi, and C. da Silva, "Origin of the imbalance between energy cascade and dissipation in turbulence," Phys. Rev. E **90**, 023003 (2014).
[43] C. R. Doering and C. Foias, "Energy dissipation in body-forced turbulence," J. Fluid Mech. **467**, 289–306 (2002).
[44] C. Meneveau and J. Katz, "Scale-invariance and turbulence models for large-eddy simulations," Annu. Rev. Fluid Mech. **32**, 1–32 (2000).
[45] U. Piomelli, W. H. Cabot, P. Moin, and S. Lee, "Subgridscale backscatter in turbulent and transitional flows," Phys. Fluids A **3**, 1766 (1991).
[46] A. Groisman and V. Steinberg, "Elastic turbulence in a polymer solution flow," Nature **405**, 53–55 (2000).
[47] W. D. McComb, J. Allan, and C. A. Greated, "Effect of polymer additives on the small-scale structure of grid-generated turbulence," Phys. Fluids **20**, 873 (1977).
[48] E. van Doorn, C. White, and K. R. Sreenivasan, "The decay of grid turbulence in polymer and surfactant solutions," Phys. Fluids **11**, 2387 (1999).
[49] S. Berti, A. Bistagnino, G. Boffetta, A. Celani, and S. Musacchio, "Small-scale statistics of viscoelastic turbulence," Europhys. Lett. **76**, 63–69 (2006).
[50] P. Perlekar, D. Mitra, and R. Pandit, "Manifestations of drag reduction by polymer additives in decaying, homogeneous, isotropic turbulence," Phys. Rev. Lett. **97**, 264501 (2006).
[51] A. Robert, T. Vaithianathan, L. Collins, and J. G. Brasseur, "Polymer-laden homogeneous shear-driven turbulent flow: A model for polymer drag reduction," J. Fluid Mech. **657**, 189–226 (2010).
[52] A. Monin and A. Yaglom, *Statistical Fluid Mechanics* (MIT Press, 1975), Vol. 2.
[53] L. C. Cheung and T. A. Zaki, "An exact representation of the nonlinear triad interaction terms in spectral space," J. Fluid Mech. **748**, 175–188 (2014).
[54] S. L. Woodroff and R. Rubinstein, "Multiple-scale perturbation analysis of slowly evolving turbulence," J. Fluid Mech. **565**, 95–103 (2006).
[55] K. Horiuti, K. Matsumoto, and K. Fujiwara, "Remarkable drag reduction in non-affine viscoelastic turbulent flows," Phys. Fluids **25**, 015106 (2013).
[56] Q. Zhou and R. Akhavan, "A comparison of FENE and FENE-P dumbbell and chain models in turbulent flow," J. Non-Newtonian Fluid Mech. **109**, 115–155 (2003).
[57] M. Herrchen and H. Öttinger, "Calculation of viscoelastic flow using molecular models: The CONNFFESSIT approach," J. Non-Newtonian Fluid Mech. **68**, 1–20 (1997).
[58] R. Keunings, "On the Peterlin approximation for finitely extensive dumbbells," J. Non-Newtonian Fluid Mech. **68**, 85–100 (1997).
[59] P. Doyle, E. Shaqfeh, G. McKinley, and S. Spiegelberg, "Relaxation of dilute polymer solutions following extensional flow," J. Non-Newtonian Fluid Mech. **76**, 79–110 (1998).
[60] G. Lielens, P. Halin, I. Jaumain, R. Keunings, and V. Legat, "New closure approximations for the kinetic theory of finitely extensible dumbbells," J. Non-Newtonian Fluid Mech. **76**, 249–279 (1998).

Reuse of AIP Publishing content is subject to the terms at: https://publishing.aip.org/authors/rights-and-permissions. Downloaded to IP: 193.136.33.229 On: Fri, 22 Jul 2016 15:24:55